Volume 11
Number 7
21 February 2023
Pages 3157–3736

Journal of Materials Chemistry A

Materials for energy and sustainability

rsc.li/materials-a

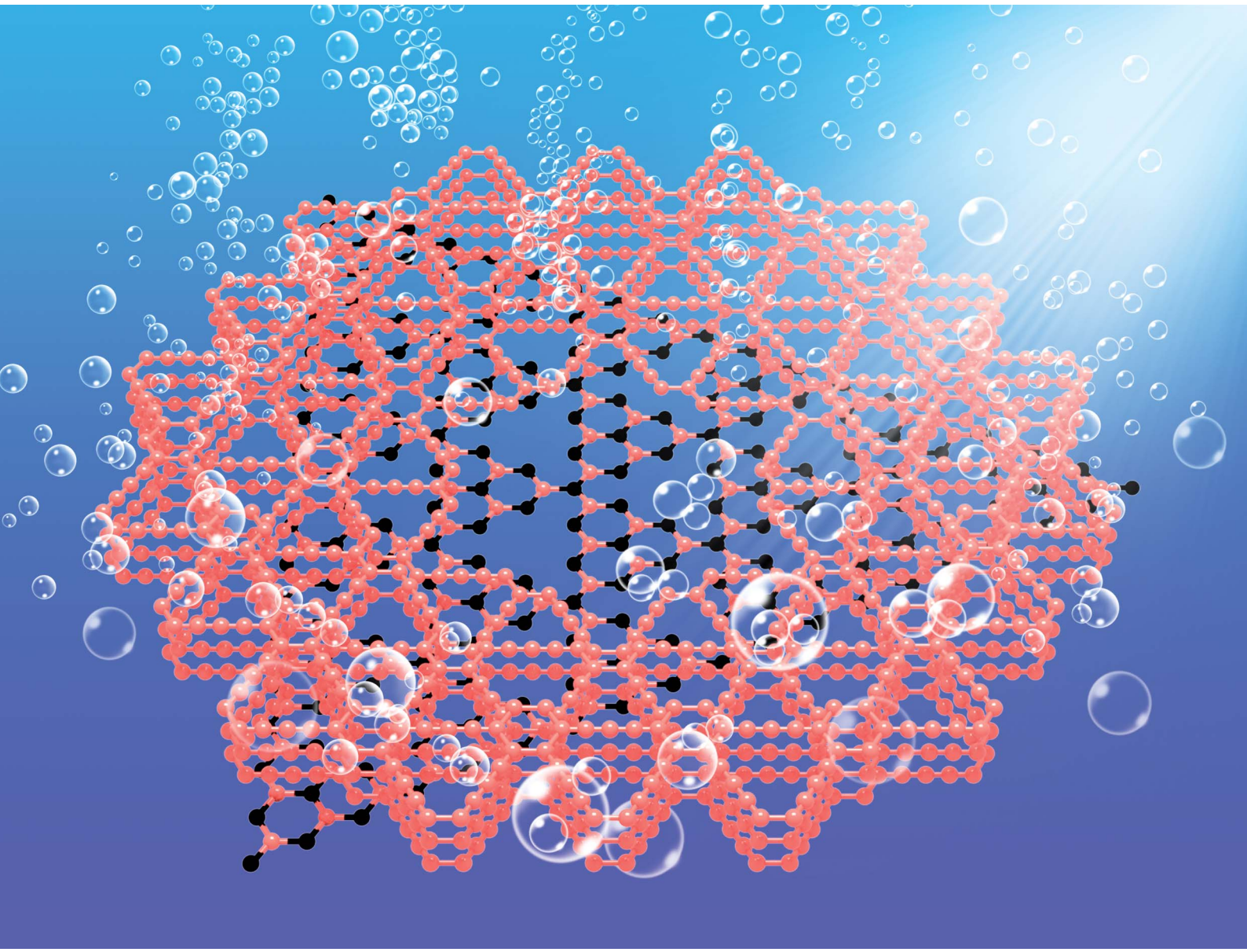

ISSN 2050-7488

ROYAL SOCIETY OF CHEMISTRY

PAPER

Mohamed Nawfal Ghazzal, Jian Li *et al.*

In situ construction of graphdiyne based heterojunctions by a deprotection-free approach for photocatalytic hydrogen generation

10 YEARS ANNIVERSARY

Journal of Materials Chemistry A

ROYAL SOCIETY OF CHEMISTRY

PAPER

View Article Online
View Journal | View Issue

Cite this: J. Mater. Chem. A, 2023, 11, 3380

In situ construction of graphdiyne based heterojunctions by a deprotection-free approach for photocatalytic hydrogen generation†

Cong Wang,‡[a] Xu Han,‡[b] Qian Xu,[a] Yi-Ning Sun,[c] Jordi Arbiol,[bd] Mohamed Nawfal Ghazzal *[a] and Jian Li *[ae]

Received 21st December 2022
Accepted 18th January 2023

DOI: 10.1039/d2ta09918g

rsc.li/materials-a

Graphdiyne (GDY) with a direct bandgap, high charge carrier mobility, and ordered pore structure, is considered an excellent matrix for the construction of heterojunction photocatalysts. However, the traditional fabrication methods for GDY-based heterojunctions require a complicated deprotection of hexakis-[(trimethylsilyl)ethynyl]benzene (HEB-TMS) and usually result in localized heterojunctions. Herein, we developed a facile deprotection-free method to *in situ* grow GDY on the surface of C_3N_4 by directly using HEB-TMS as the precursor. Such a method enabled the formation of an integral GDY@C_3N_4 heterojunction, resulting in a significantly enhanced photocatalytic activity in the visible region. The optimized GDY@C_3N_4 showed 15.6-fold hydrogen production efficiency compared to pristine C_3N_4, and outperformed the GDY/C_3N_4 samples synthesized by other approaches (*e.g.* physical mixing, hydrothermal treatment and calcination treatment). This study provides a universal and efficient strategy for the design of GDY-based heterojunction photocatalysts for solar-to-hydrogen energy conversion.

1 Introduction

Photocatalytic solar-to-hydrogen energy conversion is one of the most promising technologies to simultaneously solve global environmental issues and energy crises.[1–4] Along with the intensive research in the development of efficient and cost-effective photocatalysts,[5–7] carbon-based heterojunction photocatalysts have emerged as a new class of alternative materials.[6] Graphdiyne (GDY), consisting of both sp^2 and sp hybridized carbons, is a rising-star 2D carbon material.[8–10] Different from zero-bandgap graphene, GDY possesses the characteristics of a semiconductor with a direct band gap, suitable band energy levels and comparable intrinsic charge carrier mobility, which enable the occurrence of efficient photocatalytic reactions.[11] Furthermore, the large surface area and porous structure of GDY provide huge adsorption sites for reactants and promote the mass transfer in the in-plane and out-of-plane directions efficiently.[12] All these fascinating features make GDY an excellent host matrix to construct heterojunction photocatalysts.[13–15]

So far, a variety of GDY-based heterojunction photocatalysts have been prepared, such as GDY/TiO_2,[16–19] GDY/CdS,[20] GDY/C_3N_4,[21–26] *etc.* These heterojunction systems were constructed by a hydrothermal method, calcination, or physical adsorption. In these processes, GDY was firstly synthesized on Cu substrates and the exfoliated GDY powder was then hybridized with other semiconductors, which is time-consuming and usually results in localized heterojunctions. Very recently, some GDY-based heterojunctions were fabricated by directly growing GDY on the other semiconductors including CuI/GDY,[27] CuBr/GDY[28] and $NiTiO_3$/CuI/GDY,[29] enabling GDY to uniformly cover other semiconductors. However, the reported *in situ* growth method is limited to Cu-based semiconductors and requires the pre-synthesis of hexaethynylbenzene (HEB) monomer *via* a complex deprotection of hexa[(trimethylsilyl)ethynyl]benzene (HEB-TMS). To the best of our knowledge, no attempt has been reported to *in situ* grow GDY on other semiconductors by directly using HEB-TMS as the precursor.

With this in mind, a straightforward deprotection-free method using HEB-TMS as the monomer for the *in situ* growth of GDY on the surface of C_3N_4 was developed. The uniform coating of GDY on C_3N_4 led to an integral GDY@C_3N_4 heterojunction, which greatly improved the photocatalytic activity in the visible region. As a result, the optimized GDY@C_3N_4 displayed a 15.6-fold hydrogen production efficiency compared to pure C_3N_4. Compared to the GDY/C_3N_4

[a]Institut de Chimie Physique, UMR 8000 CNRS, Université Paris-Saclay, 91405 Orsay, France. E-mail: mohamed-nawfal.ghazzal@universite-paris-saclay.fr; jian.li@epfl.ch
[b]Catalan Institute of Nanoscience and Nanotechnology (ICN2), CSIC and BIST, Campus UAB, Bellaterra, 08193, Barcelona, Catalonia, Spain
[c]McGill University, 845 Rue Sherbrooke O, H3A 0G4, Canada
[d]ICREA, Pg. Lluís Companys 23, 08010 Barcelona, Catalonia, Spain
[e]Laboratory of Renewable Energy Science and Engineering, Institute of Mechanical Engineering, EPFL, Station 9, 1015 Lausanne, Switzerland

† Electronic supplementary information (ESI) available. See DOI: https://doi.org/10.1039/d2ta09918g

‡ These authors contributed equally to this work.

samples prepared by physical mixing, hydrothermal treatment and calcination treatment, the as-prepared GDY@C_3N_4 exhibited the best photocatalytic performance, further confirming the superiority of this strategy. This simple and effective method can be easily extended to other GDY-based heterojunctions, offering a promising strategy for the rational design of novel photocatalysts.

2 Materials and methods

2.1 Materials

All solvents and reagents including urea (Sigma-Aldrich), hexakis[(trimethylsilyl) ethynyl]benzene (HEB-TMS, purchased from Nanjing XFNANO Materials Tech Co., Ltd), tetrahydrofuran (THF, Sigma-Aldrich), *N*,*N*-dimethylformamide (DMF, Sigma-Aldrich), ethyl acetate (EA, Sigma-Aldrich), tetrabutylammonium fluoride (TBAF, 1 M in THF, Sigma-Aldrich), hydrochloric acid (HCl, 37%, Sigma-Aldrich), triethanolamine (TEOA, Sigma-Aldrich), ethanol (Sigma-Aldrich), methanol (Sigma-Aldrich), ultra-pure water (Millipore System, 18.2 MΩ cm), copper(I) chloride (CuCl, Sigma-Aldrich), chloroplatinic acid ($H_2PtCl_6 \cdot xH_2O$, Sigma-Aldrich) and sodium sulfate (Na_2SO_4, Sigma-Aldrich) were used without further purification.

2.2 Preparation of C_3N_4 nanosheets

Typically, urea (20 g) was placed in a crucible with a lid and then calcined at 550 °C min^{-1} for 3 h in air (at the rate of 2 °C min^{-1}) to obtain bulk polymeric C_3N_4. The bulk polymeric C_3N_4 was milled into a powder in a mortar. Afterwards, the as-prepared C_3N_4 powder was thermally oxidized and etched in air at 550 °C for 4 h with a rate of 5 °C min^{-1} to yield pale yellow C_3N_4 nanosheets.

2.3 Preparation of GDY@C_3N_4 and GDY/C_3N_4

GDY was grown *in situ* on C_3N_4 through a deprotection-free method.[17] Briefly, 50 mg C_3N_4 nanosheets were sonicated for 20 min to evenly disperse in 10 mL DMF. Then, CuCl (10 mg) and an appropriate amount of HEB-TMS were added. Afterwards, the bottle was sealed and heated to 60 °C with stirring in an oil-bath for 24 h. After reaction, the sample was washed with fresh DMF, THF, methanol and ethanol sequentially. Finally, the sample was dried in the oven overnight and a brown powder was obtained. The GDY coated C_3N_4 (GDY@C_3N_4) was obtained by stirring in 1 M HCl for 6 hours to remove the CuO. By controlling the amount of HEB-TMS added, the mass ratio of HEB-TMS to C_3N_4 was set to 0.5, 1, 2, and 5%, and the prepared samples were denoted as GDY@C_3N_4-x (x = 1, 2, 3, and 4), respectively.

As reference samples, different GDY/C_3N_4 heterojunction photocatalysts were also prepared according to the previous literature.[21,22] GDY was prepared following a previously reported approach.[30] Then, 30 mg C_3N_4 and 0.3 mg GDY were dispersed in 10 mL mixture of water and ethanol ($v:v$ = 1 : 1), followed by sonication for 20 min and stirring for 1 h to obtain homogeneous suspensions. Thereafter, suspension-A was stirred continuously at room temperature for another 23 h to obtain GDY/C_3N_4-Mix. Suspension-B was transferred to a 20 mL Teflon and heated at 120 °C for 3 h to synthesize GDY/C_3N_4-Hyd. Suspension-C was evaporated at 60 °C and then was calcined at 400 °C for 2 h (with a rate of 5 °C min^{-1}) to obtain GDY/C_3N_4-Cal.

All the as-prepared photocatalysts were deposited with 1 wt% Pt through a photoreduction method before photocatalytic tests. Briefly, 30 mg photocatalyst was sonicated for 20 min to evenly disperse it in 10 mL ethanol, then a certain volume of H_2PtCl_6 solution (1 mM in ethanol) was added to the photocatalyst suspension and vigorously stirred for 30 min. Subsequently, the mixture was exposed under a xenon 300 W lamp and kept stirring for 30 min to yield photocatalysts loaded with Pt nanoparticles. Finally, the samples were washed with ethanol several times and dried in the oven at 60 °C overnight.

3 Results and discussion

As shown in Fig. 1a, the *in situ* growth of GDY on C_3N_4 was achieved through a simple deprotection-free strategy by employing CuCl and DMF as the catalyst and solvent, respectively. Due to the large amount of amino groups, the surface of C_3N_4 tends to be negatively charged, which facilitates the adsorption of Cu^+ ions on its surface. It has been demonstrated that Cu^+ ions in DMF can promote the coupling reaction of HEB-TMS,[17] thus allowing the formation of a uniform GDY layer on the C_3N_4 surface. Ultimately, the CuO generated during the process was removed by using 1 M HCl to yield GDY@C_3N_4 powders. The morphology of as-prepared C_3N_4 and GDY@C_3N_4 was investigated by high-angle annular dark field scanning transmission electron microscopy (HAADF-STEM). Numerous ultrathin and overlapping filamentous structures were observed in Fig. 1b and S1,† indicating that the C_3N_4 was successfully stripped into layers after secondary thermal oxidation and etching in air. The coating of GDY brought no structural changes to C_3N_4 but modified the color from the original pale yellow to brown, which darkens with increased usage of the HEB-TMS precursor (Fig. 1b–d and S2†).

To further reveal the microstructure of C_3N_4 and GDY@C_3N_4, transmission electron microscopy (TEM) measurements were carried out. As displayed in Fig. 2a, b and S3,† C_3N_4 showed curled edges and an abundance of pores with size of several tens of nanometers. The formation of these pores may originate from gas emissions during the thermal polymerization of urea, which contributes to the diffusion of the reactants.[31] The elemental composition mapping of C_3N_4 was determined by electron energy loss spectroscopy (EELS) from the red square region in the HAADF-STEM micrograph (Fig. 2c). It can be seen that the C_3N_4 nanosheets showed a uniform distribution of C and N elements throughout the structure, although C_3N_4 and GDY were not easily distinguished in TEM images due to the similar atomic numbers of C and N as well as the amorphous property. Compared with the pristine C_3N_4, two different components can be clearly observed from the TEM image of GDY@C_3N_4, including the curled filamentary C_3N_4 and the flattened thinner flakes of GDY (Fig. 2d, e and S4†). In contrast to previous reports,[21–23] GDY was evenly adhered

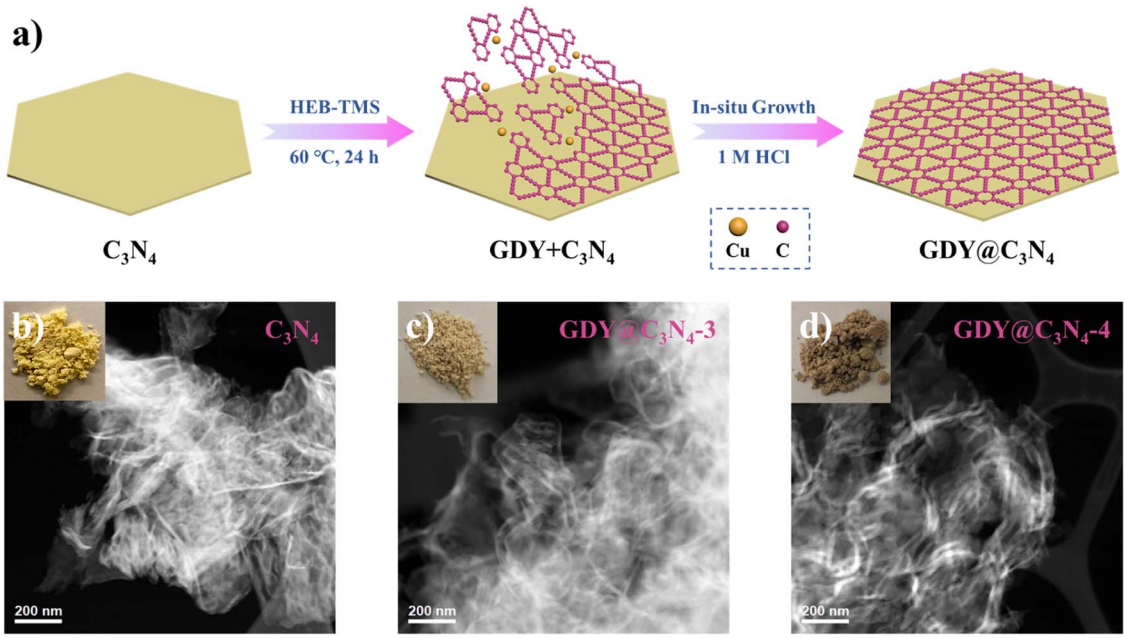

Fig. 1 (a) Schematic illustration for the preparation of GDY@C_3N_4 *via* a one-pot method. Photographs of samples and corresponding HAADF-STEM images of (b) C_3N_4, (c) GDY@C_3N_4-3, (d) GDY@C_3N_4-4.

around the C_3N_4 rather than forming only regional interfaces, suggesting an omnidirectional growth of GDY on the surface of C_3N_4. This view was further confirmed by the EELS mapping of the GDY@C_3N_4. Fig. 2f shows a homogeneous elemental distribution of C and N, where there was an obvious expansion of the C distribution on GDY@C_3N_4, which indicated the

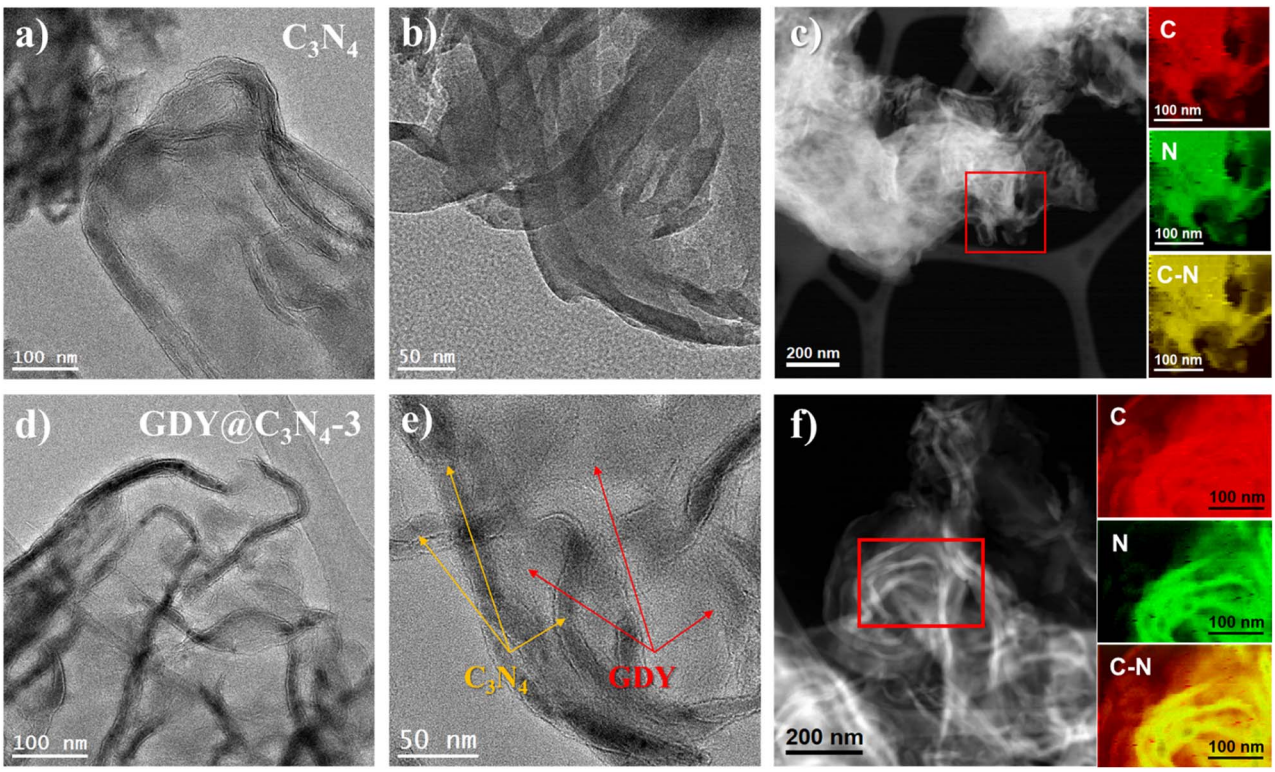

Fig. 2 TEM images showing the morphology of (a and b) C_3N_4 and (d and e) GDY@C_3N_4-3. (Yellow arrows point to the darker curly filamentous areas, belonging to C_3N_4. Red arrows point to the shallower flattened flake areas, belonging to GDY.) HAADF-STEM images of (c) C_3N_4 and (f) GDY@C_3N_4-3, and the corresponding representative EELS chemical composition mapping obtained from the red squared area in the STEM images. In dividual mapping obtained from the C K-edge at 284 eV (red), N K-edge at 402 eV (green) and C–N composite mapping (yellow).

successful coating of C_3N_4 by GDY. The unique encapsulation structure of GDY@C_3N_4 photocatalysts predicts excellent charge separation/transfer ability and promising photocatalytic performance can be expected.[32]

X-ray diffraction (XRD) was used to investigate the crystal structures of the synthesized samples (Fig. 3a). GDY exhibited a typical broad and weak diffraction peak centred at around 21.2°, corresponding to the characteristic (002) plane of the graphite-type carbon, which reveals a distortion of the ordered arrangement of GDY along its stacking direction.[17,33] Two obvious diffraction peaks at 13.1° and 27.4° can be observed from the XRD diagram of C_3N_4, which are assigned to the (100) plane from the interplanar stacking of the conjugate segments and the (002) plane originating from interlayer structural packing units, respectively.[7,34,35] The characteristic peaks of C_3N_4 were retained in the GDY@C_3N_4 samples, suggesting that the presence of GDY did not disrupt the crystal structure of C_3N_4. Diffraction peaks belonging to GDY cannot be detected in GDY@C_3N_4 composites due to the poor crystallinity and low content.[26] However, it is worth mentioning that the characteristic peaks corresponding to C_3N_4 decreased with increased amount of GDY, which could be attributed to the partial shielding effect of the GDY, further validating the homogeneous growth of the GDY. The chemical composition of GDY@C_3N_4 was analyzed by X-ray photoelectron spectra (XPS). The XPS general survey indicated the presence of C, N and O (Fig. S5†). No peaks attributed to Cu were observed, which suggested the complete removal of Cu after acid treatment (Fig. S6†). The high-resolution C 1s XPS spectra of GDY@C_3N_4 display four sub-peaks (Fig. 3b), where the peaks located at 284.5 and 286.0 eV can be assigned to C=C (sp^2) and C–O, while the peaks at 287.5 and 288 eV can be attributed to C–N (sp^2) in C_3N_4, respectively.[21,36–39] The N 1s XPS spectra of GDY@C_3N_4 can also be deconvoluted into four sub-peaks at 399.1 eV for sp^2-hybridized N in the C–N heterocycle (C=N–C), 400.7 eV for sp^3-hybridized N (N–C_3), 401.7 eV for amino groups (–NH) and 405.1 eV for charge effects, respectively (Fig. 3c).[40–42] Fourier-transform infrared (FT-IR) spectroscopy was conducted to further examine the functional groups of as-prepared samples (Fig. 3d and e). The peaks located at 1381 and 1610 cm^{-1} in GDY were assigned to the stretching vibrations of C–C/C–O bonds and the skeletal vibrations of the aromatic ring, respectively.[30] A series of peaks can be observed in the range of 1200–1700 cm^{-1} in pristine C_3N_4 ascribed to the typical stretching vibrations of C–N heterocycles, while the peak located at 805 cm^{-1} can be attributed to the characteristic breathing mode of s-triazine units.[43] In addition, several broad peaks in the range 3000–3400 cm^{-1} are designated as the stretching vibrations for amino groups.[44] No significant changes were observed in the FT-IR spectra of GDY@C_3N_4, indicating that the *in situ* growth of GDY has no effect on the structure of C_3N_4. Similarly, no distinct peaks belonging to GDY can be observed in the GDY@C_3N_4 samples due to the peak overlap between the C–N heterocycle and aromatic ring as well as the low content of GDY, which is consistent with the XRD results. Of note, the peaks belonging to C–N heterocycles shifted to higher wavenumbers in GDY@C_3N_4 compared to the pure C_3N_4, indicating a strong interaction between GDY and C_3N_4 (Fig. 3e). This result demonstrates the formation of chemical bonds and heterojunctions between C_3N_4 and GDY, which serves as charge

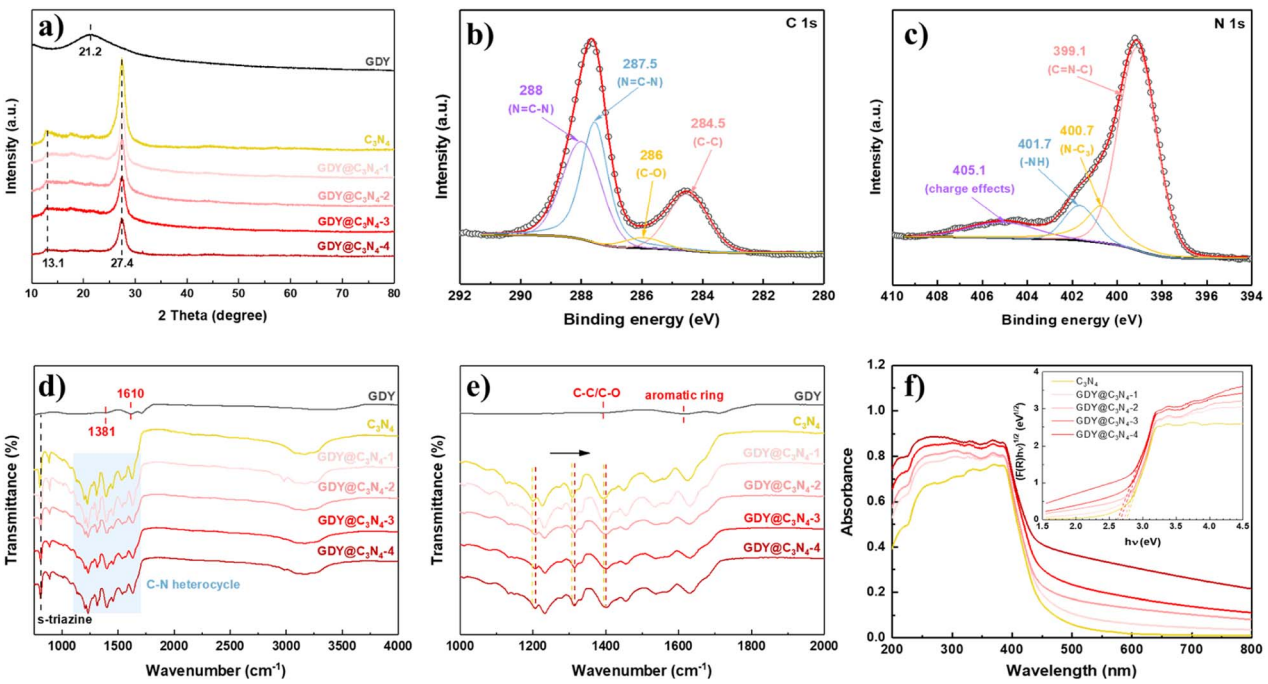

Fig. 3 (a) XRD patterns of the prepared samples. High resolution XPS spectra of GDY@C_3N_4: (b) C 1s and (c) N 1s. (d) FT-IR spectra of prepared samples. (e) Enlarged FT-IR spectra from (d). (f) UV-vis diffuse reflectance spectra of prepared samples (inset is the corresponding Kubelka–Munk plot).

transfer channels to enhance the photocatalytic performance.[21,37,45]

To evaluate the light absorption capacity of the as-prepared samples, UV-vis diffuse reflectance spectroscopy (DRS) was carried out. Compared to pure C_3N_4, the introduction of GDY significantly improves the absorption in the visible region owing to its excellent visible light absorption, and the intensity simultaneously enhances with the increased amount of GDY.[25] The optical bandgaps were estimated through the Kubelka–Munk (K–M) method, where the bandgap of C_3N_4 was determined to be 2.7 eV, while the bandgap for GDY@C_3N_4 samples reduced to 2.6 eV. The strong visible light absorption and narrow bandgap make GDY@C_3N_4 a promising visible-light driven photocatalyst.

The photocatalytic activities of C_3N_4 and GDY@C_3N_4 were estimated towards the hydrogen evolution reaction (HER) under visible light illumination (>420 nm), employing 1 wt% of Pt as a cocatalyst. Triethanolamine was used as the sacrificial reagent to deplete the photogenerated holes. The photocatalytic H_2 production rate of C_3N_4, which showed negligible H_2 generation, was significantly improved when covered by GDY. The photocatalytic activity increased with the content of GDY and reached an optimal photoactivity of 798 μmol g^{-1} h^{-1} for GDY@C_3N_4-3/Pt (Fig. 4d and S7†), exceeding that of C_3N_4/Pt by approximately 15.6-fold. A further increase in GDY reduced the H_2 evolution rate, probably because an excessively thick GDY layer disrupts the delicate balance between photogenerated carrier separation and light utilization efficiency (Fig. 4a–c).[21] In addition, no significant deactivation was observed after four consecutive cycles, implying the robust stability of GDY@C_3N_4-3/Pt (Fig. 4e). Such enhancement in photocatalytic performance and high stability is attributed to the excellent conductivity and protection of the GDY layer, which can effectively facilitate the transfer of photogenerated carriers and also can inhibit the photocorrosion.[46,47]

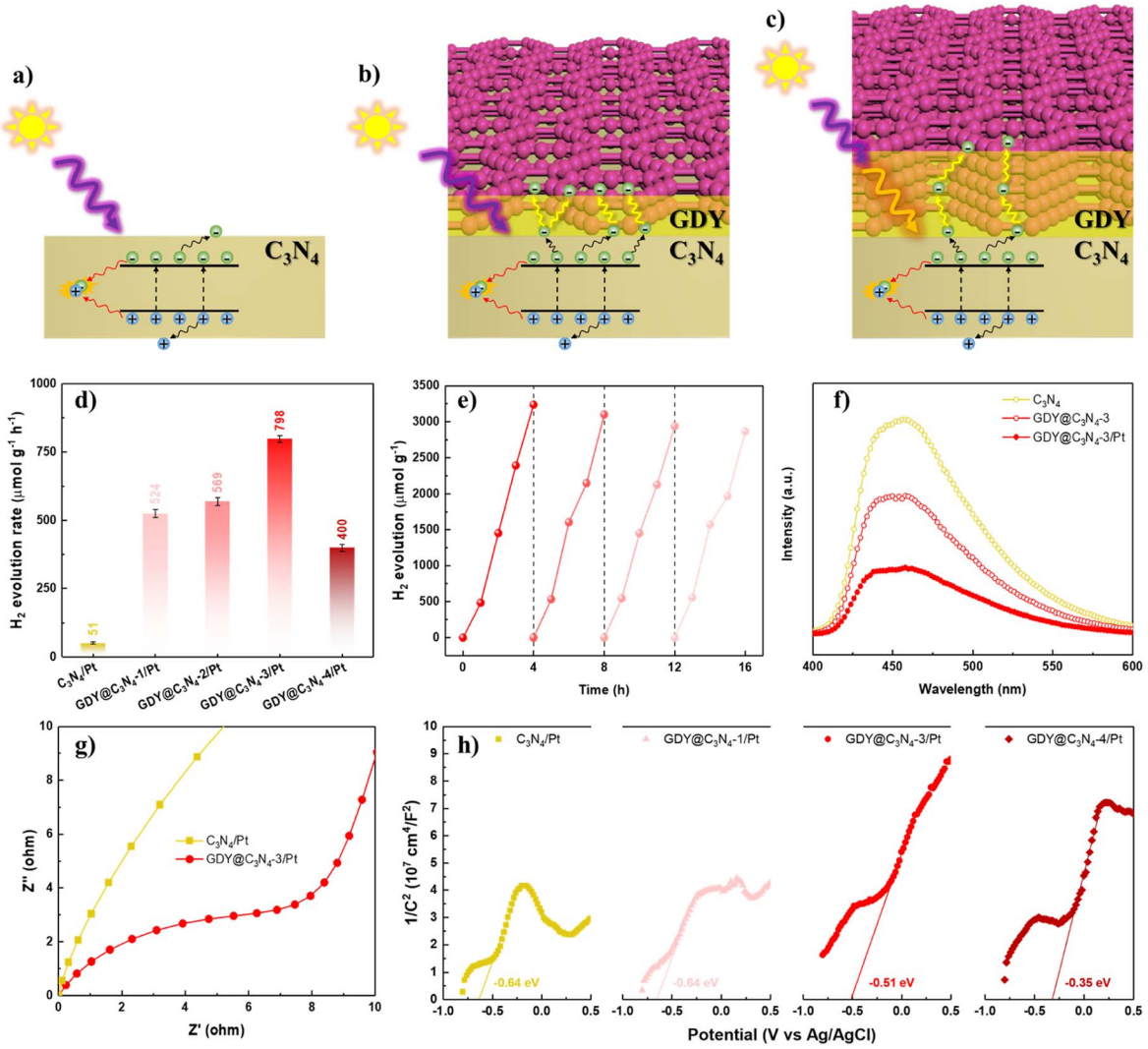

Fig. 4 (a–c) Schematic illustrations of the charge transfer pathways on the C_3N_4 and GDY@C_3N_4. (d) H_2 evolution rate of as-prepared photocatalysts under visible light (λ > 420 nm). (e) Long-term HER test with GDY@C_3N_4-3/Pt. (f) PL spectra of C_3N_4, GDY@C_3N_4-3 and GDY@C_3N_4-3/Pt. (g) EIS Nyquist plots of C_3N_4/Pt and GDY@C_3N_4-3/Pt in the dark. (h) MS plots of C_3N_4/Pt and GDY@C_3N_4/Pt composites.

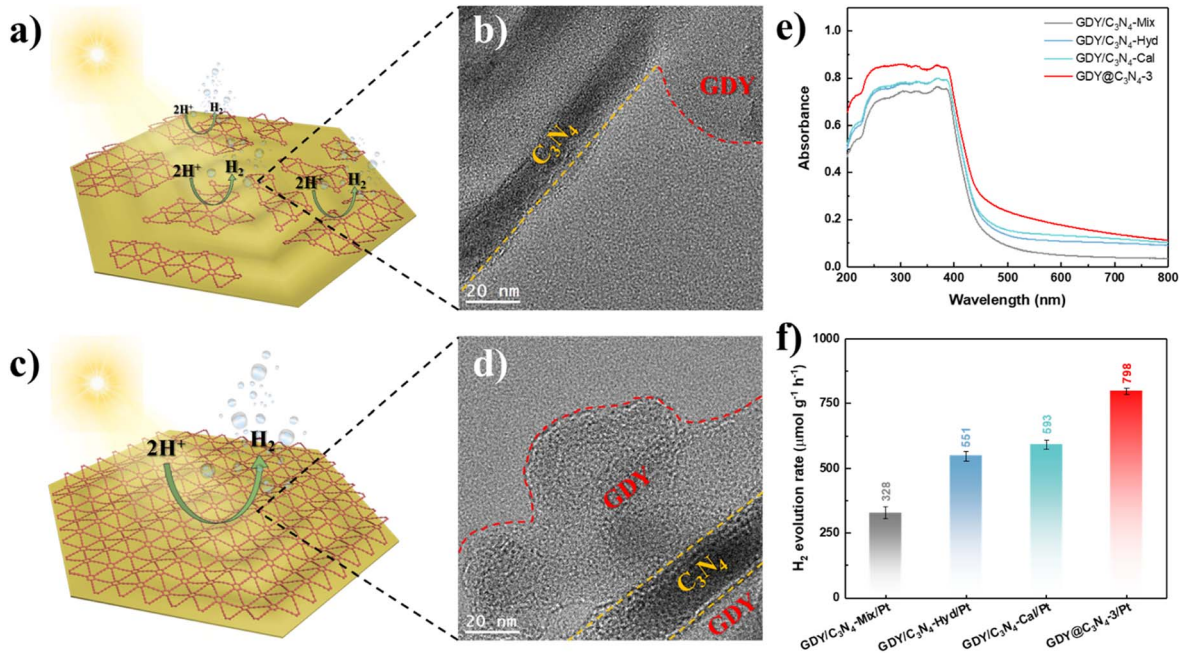

Fig. 5 (a) Schematic diagram of GDY/C_3N_4-Hyd and (b) corresponding TEM image. (c) Schematic diagram of GDY@C_3N_4-3 and (d) corresponding TEM image. (e) UV-vis diffuse reflectance spectra of GDY@C_3N_4-3 and GDY/C_3N_4 samples. (f) H_2 evolution rate of GDY@C_3N_4-3/Pt and GDY/C_3N_4/Pt photocatalysts under visible light (λ > 420 nm).

To further validate the role of the GDY layer in the GDY@C_3N_4 heterojunction, photoluminescence (PL) spectroscopy and photoelectrochemical measurements were carried out. As exhibited in Fig. 4f, GDY@C_3N_4-3 showed an obvious PL quenching compared with pure C_3N_4, which suggested that GDY could efficiently extract the photogenerated carriers from C_3N_4.[48] The introduction of Pt nanoparticles further facilitated charge carrier separation. Electrochemical impedance spectroscopy (EIS) was performed to reveal the charge carrier transfer capability.[49] The smaller radius of curvature for GDY@C_3N_4-3/Pt indicated a lower charge transfer resistance than C_3N_4/Pt (Fig. 4g). Mott–Schottky (MS) measurements were employed to evaluate the band structure of the photocatalysts.[50,51] All the MS plots showed positive slopes, indicating that both C_3N_4/Pt and GDY@C_3N_4/Pt are n-type semiconductors (Fig. 4h). Compared to C_3N_4/Pt, there was a positive shift of −0.29 V in the flat-band potential of GDY@C_3N_4/Pt samples, and more positive shift was observed with increased GDY content. This positive shift can be attributed to the construction of an internal electric field at the GDY–C_3N_4 interface, which is beneficial for the separation of photogenerated carriers, consistent with previous results.[52]

Based on the above-mentioned results, the *in situ* growth of GDY on the surface of C_3N_4 is an effective method for enhancing its photocatalytic activity. To further demonstrate the superiority of this strategy, three samples were synthesized using physical mixing, hydrothermal treatment and calcination treatment according to previous studies, namely GDY/C_3N_4-Mix, GDY/C_3N_4-Hyd and GDY/C_3N_4-Cal, respectively.[21,22] C_3N_4 still maintained the same filamentous morphology after treatments due to its thermal stability (Fig. S8†). Although these methods can achieve the hybridization of GDY with C_3N_4 through the π–π stacking interaction, the formed GDY/C_3N_4 heterojunction exhibited locality, which may be filled in the voids of C_3N_4 or partially attached to its surface (Fig. 5a, b and S9†). The EELS mappings of GDY/C_3N_4-Hyd and GDY/C_3N_4-Cal showed a homogeneous elemental distribution of C and N, indicating that most of the GDY was present in the voids of C_3N_4 and cannot be distinguished (Fig. S10†). These results are strikingly different from those observed in GDY@C_3N_4 samples, which achieved a complete coating of GDY on C_3N_4 (Fig. 5c, d and 2f). The GDY/C_3N_4 samples with localized heterojunctions displayed lower light absorption capability and H_2 generation efficiency compared with the uniformly coated GDY@C_3N_4 sample (Fig. 5e, f and S11). Therefore, the *in situ* growth of GDY enabled an integral GDY@C_3N_4 heterojunction instead of localized heterojunctions, which maximizes the advantages of GDY to promote the photogenerated carrier separation and transfer efficiently.

4 Conclusions

In summary, we have developed a deprotection-free strategy directly using HEB-TMS as a precursor to *in situ* grow GDY on C_3N_4. This one-pot method realized the uniform coating of GDY, which efficiently promotes the photogenerated carrier separation/transfer and greatly improves the photocatalytic activity in the visible region. The optimized GDY@C_3N_4 achieved 15.6-fold hydrogen production efficiency compared to pure C_3N_4. Moreover, the as-prepared GDY@C_3N_4 exhibited much better photocatalytic activity than the GDY/C_3N_4 samples constructed by physical mixing, hydrothermal treatment and

calcination treatment, further demonstrating the excellence of this approach. This work provides a facile and universal strategy for the design of GDY-based heterojunctions for photocatalytic hydrogen generation.

Conflicts of interest

There are no conflicts to declare.

Acknowledgements

ICN2 acknowledges funding from Generalitat de Catalunya 2017 SGR 327. ICN2 is supported by the Severo Ochoa program from Spanish MINECO (Grant No. SEV-2017-0706). C. W and M. N. G. acknowledge the public grant overseen by the French National Research Agency (ANR) as part of the ERANET-ACT3 call program and the Paris Ile-de-France Region (DIM RESPORE-2021-27) for financial support. MNG thanks the French National Research Agency (ANR), through the Ingen Cat project (ANR-20-CE43-0014), for the financial support.

References

1 H. Nishiyama, T. Yamada, M. Nakabayashi, Y. Maehara, M. Yamaguchi, Y. Kuromiya, Y. Nagatsuma, H. Tokudome, S. Akiyama, T. Watanabe, R. Narushima, S. Okunaka, N. Shibata, T. Takata, T. Hisatomi and K. Domen, *Nature*, 2021, **598**, 304–307.
2 T. Takata, J. Jiang, Y. Sakata, M. Nakabayashi, N. Shibata, V. Nandal, K. Seki, T. Hisatomi and K. Domen, *Nature*, 2020, **581**, 411–414.
3 C. Wang, B. Weng, Y. Liao, B. Liu, M. Keshavarz, Y. Ding, H. Huang, D. Verhaeghe, J. A. Steele, W. Feng, B. L. Su, J. Hofkens and M. B. J. Roeffaers, *Chem. Commun.*, 2022, **58**, 10691–10694.
4 C. Wang, J. Li, E. Paineau, A. Laachachi, C. Colbeau-Justin, H. Remita and M. N. Ghazzal, *J. Mater. Chem. A*, 2020, **8**, 10779–10786.
5 X. Yuan, C. Wang, D. Dragoe, P. Beaunier, C. Colbeau-Justin and H. Remita, *Appl. Catal., B*, 2021, **281**, 119457.
6 M. Z. Rahman, M. G. Kibria and C. B. Mullins, *Chem. Soc. Rev.*, 2020, **49**, 1887–1931.
7 X. Wang, K. Maeda, A. Thomas, K. Takanabe, G. Xin, J. M. Carlsson, K. Domen and M. Antonietti, *Nat. Mater.*, 2009, **8**, 76–80.
8 J. Li, X. Gao, L. Zhu, M. N. Ghazzal, J. Zhang, C.-H. Tung and L.-Z. Wu, *Energy Environ. Sci.*, 2020, **13**, 1326–1346.
9 Y. Fang, Y. Liu, L. Qi, Y. Xue and Y. Li, *Chem. Soc. Rev.*, 2022, **51**, 2681–2709.
10 X. Gao, J. Li, R. Du, J. Zhou, M.-Y. Huang, R. Liu, J. Li, Z. Xie, L.-Z. Wu, Z. Liu and J. Zhang, *Adv. Mater.*, 2017, **29**, 1605308.
11 Y. Jiao, A. Du, M. Hankel, Z. Zhu, V. Rudolph and S. C. Smith, *Chem. Commun.*, 2011, **47**, 11843–11845.
12 C. Huang, Y. Li, N. Wang, Y. Xue, Z. Zuo, H. Liu and Y. Li, *Chem. Rev.*, 2018, **118**, 7744–7803.
13 S. Liang, H. Deng, Z. Zhou and W. Y. Wong, *EcoMat*, 2022, e12297, DOI: **10.1002/eom2.12297**.
14 F. Xu, K. Meng, B. Zhu, H. Liu, J. Xu and J. Yu, *Adv. Funct. Mater.*, 2019, **29**, 1904256.
15 J. Li, X. Gao, B. Liu, Q. Feng, X. B. Li, M. Y. Huang, Z. Liu, J. Zhang, C. H. Tung and L. Z. Wu, *J. Am. Chem. Soc.*, 2016, **138**, 3954–3957.
16 J. Li, A. Slassi, X. Han, D. Cornil, M. H. Ha-Thi, T. Pino, D. P. Debecker, C. Colbeau-Justin, J. Arbiol, J. Cornil and M. N. Ghazzal, *Adv. Funct. Mater.*, 2021, **31**, 2100994.
17 J. Li, X. Han, D. Wang, L. Zhu, M. H. Ha-Thi, T. Pino, J. Arbiol, L. Z. Wu and M. Nawfal Ghazzal, *Angew. Chem., Int. Ed.*, 2022, **61**, e202210242.
18 J. Li, Z. Xie, Y. Xiong, Z. Li, Q. Huang, S. Zhang, J. Zhou, R. Liu, X. Gao, C. Chen, L. Tong, J. Zhang and Z. Liu, *Adv. Mater.*, 2017, **29**, 1700421.
19 R. Wang, M. Shi, F. Xu, Y. Qiu, P. Zhang, K. Shen, Q. Zhao, J. Yu and Y. Zhang, *Nat. Commun.*, 2020, **11**, 4465.
20 L. Zhang, Y. Wu, J. Li, Z. Jin, Y. Li and N. Tsubaki, *Mater. Today Phys.*, 2022, **27**, 100767.
21 Q. Xu, B. Zhu, B. Cheng, J. Yu, M. Zhou and W. Ho, *Appl. Catal., B*, 2019, **255**, 117770.
22 H. Si, Q. Deng, C. Yin, J. Zhou, S. Zhang, Y. Zhang, Z. Liu, J. Zhang, J. Zhang and J. Kong, *J. Alloys Compd.*, 2020, **833**, 155054.
23 K. Yang, T. Liu, D. Xiang, Y. Li and Z. Jin, *Sep. Purif. Technol.*, 2022, **298**, 121564.
24 Y. Wang, Y. Zhang, Y. Wang, C. Zeng, M. Sun, D. Yang, K. Cao, H. Pan, Y. Wu, H. Liu and R. Yang, *ACS Appl. Mater. Interfaces*, 2021, **13**, 40629–40637.
25 H.-Y. Si, C.-J. Mao, J.-Y. Zhou, X.-F. Rong, Q.-X. Deng, S.-L. Chen, J.-J. Zhao, X.-G. Sun, Y. M. Shen, W.-J. Feng, P. Gao and J. Zhang, *Carbon*, 2018, **132**, 598–605.
26 C. Sun, Y. Liu, Z. Wang, P. Wang, Z. Zheng, H. Cheng, X. Qin, X. Zhang, Y. Dai and B. Huang, *J. Alloys Compd.*, 2021, **868**, 159045.
27 Y. Li, H. Yang, G. Wang, B. Ma and Z. Jin, *ChemCatChem*, 2020, **12**, 1985–1995.
28 J. Li, M. Li, H. Li and Z. Jin, *J. Mater. Chem. C*, 2022, **10**, 2181–2193.
29 T. Yan, H. Liu and Z. Jin, *ACS Appl. Mater. Interfaces*, 2021, **13**, 24896–24906.
30 G. Li, Y. Li, H. Liu, Y. Guo, Y. Li and D. Zhu, *Chem. Commun.*, 2010, **46**, 3256–3258.
31 Y. Hou, Z. Wen, S. Cui, X. Guo and J. Chen, *Adv. Mater.*, 2013, **25**, 6291–6297.
32 X. Zhou, B. Fu, L. Li, Z. Tian, X. Xu, Z. Wu, J. Yang and Z. Zhang, *Nat. Commun.*, 2022, **13**, 5770.
33 J. He, N. Wang, Z. Cui, H. Du, L. Fu, C. Huang, Z. Yang, X. Shen, Y. Yi, Z. Tu and Y. Li, *Nat. Commun.*, 2017, **8**, 1172.
34 P. Niu, L. Zhang, G. Liu and H.-M. Cheng, *Adv. Funct. Mater.*, 2012, **22**, 4763–4770.
35 X.-L. Pu, X.-C. Yang, S.-S. Liang, W. Wang, J.-T. Zhao and Z.-J. Zhang, *J. Mater. Chem. A*, 2021, **9**, 22373–22379.
36 R. Matsuoka, R. Sakamoto, K. Hoshiko, S. Sasaki, H. Masunaga, K. Nagashio and H. Nishihara, *J. Am. Chem. Soc.*, 2017, **139**, 3145–3152.
37 Y.-Y. Han, X.-L. Lu, S.-F. Tang, X.-P. Yin, Z.-W. Wei and T.-B. Lu, *Adv. Energy Mater.*, 2018, **8**, 1702992.

38 J. Li, X. Gao, Z. Li, J. H. Wang, L. Zhu, C. Yin, Y. Wang, X. B. Li, Z. Liu, J. Zhang, C. H. Tung and L. Z. Wu, *Adv. Funct. Mater.*, 2019, **29**, 1808079.
39 J. Li, X. Gao, X. Jiang, X.-B. Li, Z. Liu, J. Zhang, C.-H. Tung and L.-Z. Wu, *ACS Catal.*, 2017, **7**, 5209–5213.
40 P. Kuang, B. Zhu, Y. Li, H. Liu, J. Yu and K. Fan, *Nanoscale Horiz.*, 2018, **3**, 317–326.
41 D. J. Martin, K. Qiu, S. A. Shevlin, A. D. Handoko, X. Chen, Z. Guo and J. Tang, *Angew. Chem., Int. Ed.*, 2014, **53**, 9240–9245.
42 L. Zhang, R. Long, Y. Zhang, D. Duan, Y. Xiong, Y. Zhang and Y. Bi, *Angew. Chem., Int. Ed.*, 2020, **59**, 6224–6229.
43 Q. Xu, C. Jiang, B. Cheng and J. Yu, *Dalton Trans.*, 2017, **46**, 10611–10619.
44 B. Wang, J. Zhang and F. Huang, *Appl. Surf. Sci.*, 2017, **391**, 449–456.
45 N. Yang, Y. Liu, H. Wen, Z. Tang, H. Zhao, Y. Li and D. Wang, *ACS Nano*, 2013, **7**, 1504–1512.
46 B. Weng, M.-Y. Qi, C. Han, Z.-R. Tang and Y.-J. Xu, *ACS Catal.*, 2019, **9**, 4642–4687.
47 Y. Shang, X. Chen, W. Liu, P. Tan, H. Chen, L. Wu, C. Ma, X. Xiong and J. Pan, *Appl. Catal., B*, 2017, **204**, 78–88.
48 Y. Guo, J. Li, Y. Yuan, L. Li, M. Zhang, C. Zhou and Z. Lin, *Angew. Chem., Int. Ed. Engl.*, 2016, **55**, 14693–14697.
49 B. Weng and Y. J. Xu, *ACS Appl. Mater. Interfaces*, 2015, **7**, 27948–27958.
50 J. Li, X. Yang, C. Ma, Y. Lei, Z. Cheng and Z. Rui, *Appl. Catal., B*, 2021, **291**, 120053.
51 X. Yuan, D. Dragoe, P. Beaunier, D. B. Uribe, L. Ramos, M. G. Méndez-Medrano and H. Remita, *J. Mater. Chem. A*, 2020, **8**, 268–277.
52 I. A. Digdaya, G. W. P. Adhyaksa, B. J. Trzesniewski, E. C. Garnett and W. A. Smith, *Nat. Commun.*, 2017, **8**, 15968.